Journal of Materials Chemistry

Cite this: J. Mater. Chem., 2011, 21, 14979

www.rsc.org/materials

PAPER

Optical and electrical properties of individual p-type ZnO microbelts with Ag dopant

Fang Fang,*[ab] Dongxu Zhao,*[c] Xuan Fang,[ab] Jinhua Li,[ab] Zhipeng Wei,[a] Shaozhuan Wang,[a] Jilong Wu[a] and Xiaohua Wang[a]

Received 5th July 2011, Accepted 28th July 2011
DOI: 10.1039/c1jm13104d

P-type ZnO microbelts were successfully synthesized by thermal diffusion of Ag in a step by step thermal annealing process. The effect of the annealing temperature on the room temperature photoluminescence (RT-PL) and current *versus* voltage (*I–V*) properties of Ag-doped ZnO microbelts were studied. With the increase of the annealing temperature, the deep-level emission (506 nm) decreased and the Ag_{Zn} related violet emission peak at 405 nm was observed. The substitution of Zn atoms by Ag atoms is unstable at high temperature, which might be a limitation for Ag as the dopant of ZnO. In our experiment, the optimal annealing temperature is 250 °C, at which the strong neutral acceptor bound exciton (A^0X) peak appeared in the low temperature-PL spectrum. Correspondingly, the conductivity type of the ZnO microbelt transformed from n to p. The symmetrical *I–V* curves exhibited slightly nonlinear behaviors. The result indicated the existence of Schottky barriers between the individual Ag-doped ZnO microbelt and the In electrodes.

The semiconductor ZnO has gained substantial interest in the research community. That material has a wide band gap of 3.37 eV and a high exciton binding energy of 60 meV, which could lead to lasing action based on exciton recombination even at room temperature.[1,2] Moreover, its hardness, optical and piezoelectric properties make it useful in ultraviolet (UV) lasers, solar cells, photocatalysts, field emitters, gas sensors, piezo-nanogenerators and so on.[3–7] Generally, the optoelectronic behaviors of semiconductors are dominated by the defects and impurities. Metal ion doping is currently an active and leading approach to further expand the applications of ZnO. Considerable works have been reported on the doping of ZnO with several dopants to tailor its electrical and optical properties. Al doping in ZnO increased its conductivity,[8] Mn-doped ZnO had ferromagnetism,[9] Ni-doped ZnO nanowire has shown considerable increase for photoluminescence.[10] Ag is a good electrical conductor with a relatively lower optical absorption coefficient in the visible region, so it is an important optical material in the visible region. Ag-doping in ZnO is able to change the opto-electronic properties of ZnO thin films and nanostructures: early research showed that Ag incorporation in ZnO reduced the donor density,[11] and the calculated formation energy was much lower for Ag_{Zn} at a substitutional site than Agi at an interstitial site,[12–14] making it an effective acceptor in ZnO. Some recent studies confirmed the p conductivity in Ag-doped ZnO.[15–18] It has also been demonstrated that the UV emission of ZnO films can be enhanced significantly *via* Ag-doping.[19,20] However, Ag-doping single p-type ZnO microstructure-based electrical and optical properties have not yet been reported.

Therefore, in this paper, p-type ZnO microbelts were obtained *via* a facile post-annealing treatment. The effect of the Ag dopant on the optical and electrical characteristics of individual ZnO microbelts was also investigated. Among all the micro- and nanostructural ZnO oxides, the belt (ribbon)-shaped structure exhibits increased electronic and optoelectronic performance because of the absence of dislocations and other line defects.[21] Moreover, the ZnO belt is regarded as an ideal system to fully understand dimensionally confined transport phenomena and may act as a valuable unit to construct micro- and nanodevices owing to their well-defined geometry.[22] The successful synthesis of the p-type micro- and nanobelts will open the door to fabricate ZnO micro- and nanobelt-based building blocks used in micro- and nanooptoelectronic devices.[23]

The ZnO microbelts were synthesized *via* a traditional chemical vapour deposition method in a horizontal tube furnace. A mixture of commercial ZnO and graphite powders in a certain weight ratio (1 : 1) was loaded in an alumina boat and served as source material (Fig. 1(a) shows the schematic diagram of the setup). Synthesis was carried out at 990 °C for 30 min (with no deliberate use of the substrate), which under a constant flow of Ar (99.99%) with the flow rate of 100 sccm. Then, the furnace was

[a]*Changchun University of Science and Technology, 7089 Wei-Xing Road, Changchun, 130022, People's Republic of China. E-mail: fangfang1982131@yahoo.com.cn; Tel: + 86-431-86176322*
[b]*International Joint Research Center for Nanophotonics and Biophotonics, 7089 Wei-Xing Road, Changchun, 130022, People's Republic of China*
[c]*Key Laboratory of Excited State Processes, Changchun Institute of Optics, Fine Mechanics and Physics, Chinese Academy of Sciences, 16 East Nan-Hu Road, Open Economic Zone, Changchun, 130033, People's Republic of China. E-mail: dxzhao2000@yahoo.com.cn*

cooled down to room temperature naturally. Transparent belt-like materials were clearly observed on the surface of the boat.

The morphology of the ZnO microbelt was investigated by a microscope (XSP-10C/10D100). The RT and LT photoluminescence (PL) measurements were performed using a He–Cd laser line of excitation wavelength at 325 nm and a micro-Raman spectrometer in a back scattering geometry configuration to detect the emission spectra, which focused on an area of diameter 10 μm and adjusted the depth of the laser focus (model: LAB-RAM-UV JobinYvon). The current–voltage (I–V) characteristic of this device was measured using a Hall measurement system (LakeShore 7707).

The average diameter of the ZnO microbelts was about 20 μm with a length of up to 1 cm. Fig. 2 shows the photo of a typical microbelt taken by a charge-coupled device (CCD) camera from the microscope. The as-grown ZnO microbelt was so long that can be readily manipulated by the conventional Ag doping methods. A thin Ag film was first deposited on the Si (100) substrate surface *via* an electron beam evaporation method. The deposited film then served as Ag source. The ZnO microbelt was put right on the top of the Ag/Si substrate, before being placed into the furnace (Fig. 1(b) shows the schematic diagram). The furnace was heated up to the designated temperature and kept at that temperature for 1 h. Finally, the Ag element was diffused into the ZnO microbelt *via* annealing the sample at air atmosphere.

Fig. 3 shows the intensity normalized at room temperature PL spectra of the as-grown ZnO microbelt and annealing samples at various temperatures (a) 150 °C; (b) 200 °C; (c) 250 °C and (d) 300 °C. Here, the same ZnO microbelt was used, and after each annealing temperature, we got one set of PL data (that means the sample will be subjected to annealing 4 times). PL is a suitable tool to determine the crystal quality and the presence of

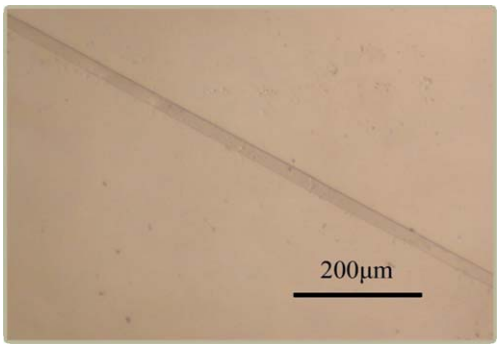

Fig. 2 The photo of a typical as-grown ZnO microbelt taken by a charge-coupled device (CCD) camera from the microscope.

impurities in the material. Generally, the PL spectrum of ZnO consisted of UV emission and the visible broadband emission. UV emission was attributed to excitonic recombination. The origin of the visible broadband emission in ZnO has not yet been clearly understood but is generally attributed to surface states, single ionized vacancies, and impurities.[24,25] As shown in Fig. 3 (a), the excellent optical properties, evident as strong excitonic emission (380 nm) and low deep level emission (506 nm), indicated that the as-grown ZnO microbelt was of high optical quality. After annealing at 150 °C, the emission band was considered as a combination of the various transitions, which could be fitted by three peaks (shown in the inset of Fig. 3), centered at $I_1 = 380$ nm, $I_2 = 405$ nm and $I_3 = 506$ nm. The peak positions I_1 and I_3 were attributed to the excitonic recombination and deep level emission from ZnO, respectively. Compared with the as-grown sample, the position of the UV emission showed no distinct change and the intensity of the I_1/I_3 peak ratio was increased. While the I_2 peak at 405 nm was not observed in any

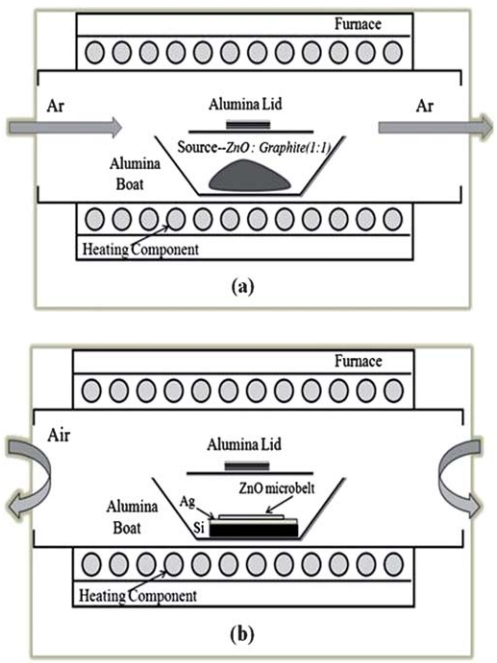

Fig. 1 The schematic diagram of the setups (a) for the growth of ZnO microbelts and (b) for Ag diffusion annealing.

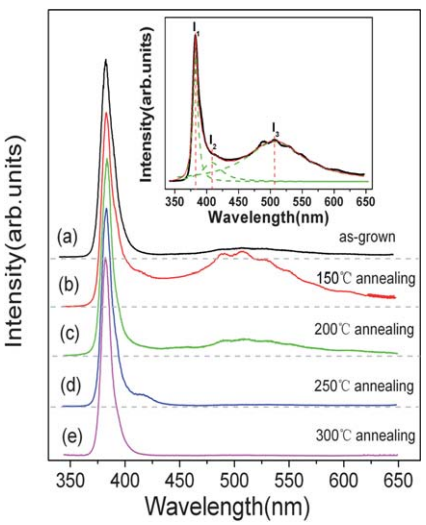

Fig. 3 PL spectra of a single ZnO microbelt measured at different annealing temperatures: (a) the as-grown ZnO microbelt; (b) the 150 °C annealing Ag doped ZnO microbelt; (c) the 200 °C annealing Ag doped ZnO microbelt; (d) the 250 °C annealing Ag doped ZnO microbelt; and (e) the 300 °C annealing Ag doped ZnO microbelt. The inset shows the curve of the 150 °C annealing sample fitted with three Gaussians (dashed lines) peaked at $I_1 = 380$ nm, $I_2 = 405$ nm and $I_3 = 506$ nm.

PL spectrum of the undoped ZnO structure, indicating that it was closely related to Ag-related impurity level transition. Gruzintsev *et al.*[26] suggested Ag could behave as an acceptor above the valence band of the ZnO. Some literature has reported the calculated formation energies are very low for Ag dopants at substitutional-Zn sites (both under low and high Ag concentrations), but rather high at substitutional-O and interstitial sites under O-rich conditions. As our Ag-doping experiment was carried out in the atmosphere (O-rich conditions), we suggested that the 405 nm emission in Fig. 3 was mainly caused by the existence of the radiative center Ag_{Zn}, which was emitted from the radiative transition between this level and the conduction band of ZnO.[27]

With the increase of temperature, the deep-level emission decreased. When the annealing temperature continues to rise to 300 °C, only the ZnO UV peak was left. It was deduced that during the initial stages of annealing, a mass of Ag was only adhered to the surface of the sample. Therefore, many surface states led to strong visible broadband emission. Also, an amount of Ag diffused into the ZnO crystal lattice, which may be evidenced by the appearance of the I_2 peak. It was related to the annealing conditions (temperature and time). As we annealed the sample step by step, when the temperature increased, the diffusion progress was slow and effective, so it was easier for Ag to diffuse into the ZnO lattice. That was consistent with the PL data shown in Fig. 3(b) and (c). With the decrease of surface states, the visible emission became weak. The I_3 peak was almost suppressed at 250 °C annealing, but the 405 nm peak still appeared. Oxygen vacancies, which commonly exist in ZnO as point defects, led to the deep-level emission.[28] The O-rich conditions also helped to restrain the visible emission. However, there must be a limitation for Ag-doped into ZnO. As the annealing temperature increased to 300 °C, a small amount of Ag atoms adhered to the surface of the sample diffused into the ZnO crystal lattice, while a large amount could diffuse into the atmosphere, meantime, Ag atoms already in the crystal lattice can escape into the atmosphere. So, only ZnO UV emission was observed in the PL spectrum.

Fig. 4 shows the *I–V* characteristics from the single ZnO microbelt (as-grown and Ag-doped) and indium (In) was used as contact electrode. In order to exclude the electrodes bringing impurities into the ZnO microbelt during the heating process, we cannot measure the *I–V* curve of one sample at different annealing temperatures just the same as the PL test. Here, we selected 5 typical as-grown samples which had similar performances following the above step by step Ag-doped annealing process: (a) as-grown; (b) 150 °C annealing; (c) 200 °C annealing (undergo 150 °C annealing); (d) 250 °C annealing (undergo 150 °C and 200 °C annealing); and (e) 300 °C annealing (undergo 150 °C, 200 °C and 250 °C annealing, respectively). The measurement results can also show the trends of contact electrical properties of ZnO and indium under different annealing temperatures.

Fig. 4(a) shows a typical ohmic contact. In such a system, the work function of In ($W_m = 4.12$ eV) was smaller than the electron-affinity of ZnO ($\chi = 4.3$ eV).[29] The as-grown ZnO was an n-type semiconductor due to its intrinsic defects. The weak deep level emission shown in Fig. 3(a) indicated that our as-grown ZnO microbelt has a low density of surface states. So there is no potential barrier between In and ZnO (a schematic energy band

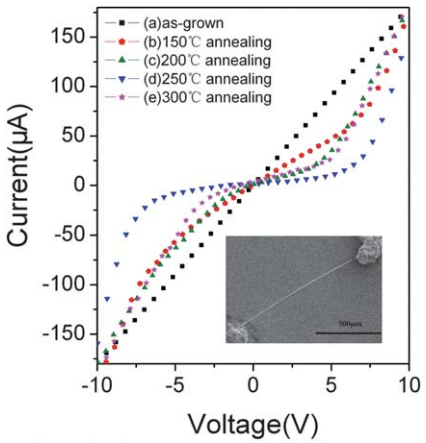

Fig. 4 *I–V* curves of individual ZnO microbelts at different annealing temperatures: (a) the as-grown ZnO microbelt; (b) the 150 °C annealing Ag doped ZnO microbelt; (c) the 200 °C annealing Ag doped ZnO microbelt; (d) the 250 °C annealing Ag doped ZnO microbelt; and (e) the 300 °C annealing Ag doped ZnO microbelt. Inset: SEM image of the ZnO microbelt device.

diagram is shown in Fig. 5(a)). But, the symmetrical *I–V* curves exhibited slightly nonlinear behaviour and the nonlinear behavior was further enhanced with the increase of the annealing temperature, which indicated the existence of barriers between the ZnO semiconductor microbelt and the metal electrodes. Interpreting measurement results in such a small scale could be tricky since a lot of uncertain elements including electrodes, contact interface and microbelt itself are involved. Particular efforts thus should be devoted to distinguish contributions from different effects before reaching the conclusion. In our doping experiment, the Ag atoms were diffused into the ZnO microbelt *via* step by step annealing. As mentioned before, the experimental conditions are conducive for Ag dopants at substitute Zn sites. Therefore, the Ag_{Zn} acting as acceptor depleted the surface electron states and reduces the free carrier density, which resulted in the space charge region and band bending of the surface. On the other hand, the 150 °C annealing sample has a mass of Ag adhered to the surface. And so many surface states can induce energy levels in the band gap and cause pinning of the Fermi level (as illustrated in Fig. 5(b)), which have a pronounced effect on the metal–semiconductor contact barriers.[30] Due to the existence of the surface states, the electrons must cross over the Schottky barrier to form a current. Diffusion is a process from the surface to the interior. With the surface states disappeared and Ag atoms gradually diffused into the ZnO crystal lattice (especially for the 250 °C annealing sample), such nonlinear behavior became prominent. We suggested that there must be a transformation from n-type to p-type for the microbelt itself (we later verified this hypothesis in the low temperature PL). Ag atoms act as acceptors, so the Fermi level of Ag-doped ZnO must move away from the bottom of the conduction band. Meanwhile, the majority carriers change from electrons to holes. Though the work functions of In and the electron-affinity of ZnO have not changed, such band bending seriously hindered the movement of the holes. Consequently, our system can be considered as a single ZnO microbelt sandwiched between two opposite Schottky

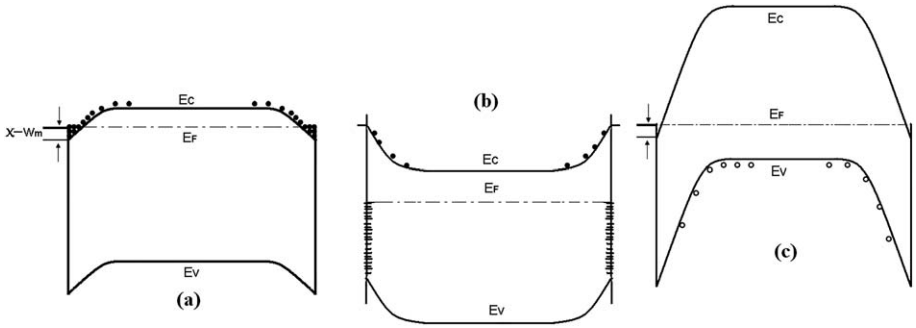

Fig. 5 Schematic energy band diagrams of ZnO surface potential with indium electrode at different conditions: (a) the as-grown ZnO microbelt; (b) the 150 °C annealing Ag doped ZnO microbelt; and (c) the 250 °C annealing Ag doped ZnO microbelt, W_m is the work functions of indium, χ is the electron-affinity of ZnO, E_C is the conduction band energy level, E_F is the Fermi level, and E_V is the valence band energy level.

diodes, as shown in the inset in Fig. 4.[29] When the temperature increased to 300 °C, a large amount of Ag elements could diffuse into the atmosphere. Compared to the 250 °C annealing sample, the contact barriers were lowered. Here, the electrical measurements were fully consistent with the PL analysis. As shown in the *I–V* curves, the Schottky barriers on both sides were slightly asymmetrical, probably due to the nonuniform diffusion of Ag-doping and uneven distribution of surface states.

In accordance with the above results, we infer that the temperature of 250 °C may be an excellent point to achieve the effective doping of Ag atoms in our experiment. To further confirm this inference, low temperature PL spectra of the 250 °C annealing sample were measured. The PL spectrum of the as-grown ZnO microbelt at 83 K is shown in Fig. 6(a). The peak located at 3.365 eV is assigned to the radiative recombination of shallow donor-bound exciton (D^0X).[31] At the high energy side of D^0X (at 3.375 eV), a small shoulder could be observed, which originated from the recombination of the free exciton (FX).[32] At the lower energy position of D^0X, three emission peaks emerged, which are considered to be the phonon replicas of FX. Here, the energy separation of FX-1LO is smaller than the LO phonon energy (72 meV) due to the energy softening of FX-1LO.[33] In addition to these phonon replicas of FX, the 250 °C annealing ZnO microbelt showed two new peaks in Fig. 6(b), which were related to Ag doping. These new peaks located at 3.353 eV and 3.32 eV were identified as an acceptor-bound exciton peak (A^0X)[34] and a free electron to neutral acceptor (e, A^0) transition at 3.323 eV,[35] respectively. This was another proof that Ag was introduced into the ZnO crystal lattice. Even though the PL measurements cannot yield information about charge carrier concentrations, the strong intensity of emission peaks associated with the acceptors reflects that the Ag-doped ZnO microbelt has successfully achieved the transition from n-type to p-type.

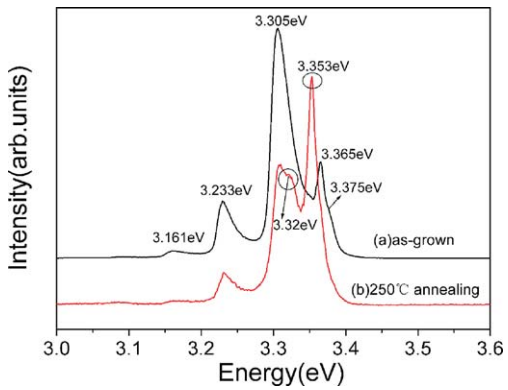

Fig. 6 Low temperature PL spectra at 83 K of the as-grown ZnO microbelt and the 250 °C annealing Ag doped ZnO microbelt.

In conclusion, Ag-doped ZnO microbelts were successfully carried out by thermal diffusion of Ag in the subsequent step by step thermal annealing process. An appropriate annealing may cause lattice relaxation and recoordination of the Ag dopants, leading to a desirable condition for effective doping. The optical and electrical properties of Ag doped ZnO microbelts were evaluated under different annealing temperatures. With the increase of the annealing temperature, Ag might displace the ideal Zn sites, which formed Ag_{Zn}-related complex defect luminescence centers, thus a new emission peak at 405 nm was observed. The substitution of Zn atoms by Ag atoms was unstable at high temperature, which might be a limitation for Ag as the dopant of ZnO. In our experiment, the optimal annealing temperature was 250 °C, at which the strong neutral acceptor bound exciton (A^0X) peak appeared in the low temperature-PL spectrum. Thus Ag acts as an acceptor in ZnO microbelts, and the conductivity type of the ZnO microbelt transformed from n to p, which makes the *I–V* characteristics in In and ZnO contact correspond to the transformation from ohmic to Schottky. All these suggest that Ag is a promising dopant in the preparation of p-type ZnO.

Acknowledgements

This work is supported by the National Natural Science Foundation of China (61006065, 61076039, 10804071), the Program for New Century Excellent Talents in University (NCET-07-022), the Project of Science Development Planning of Jilin Province (20080331-1, 20090139, 20090555), the Natural Science Foundation of Jilin Province (20101546), Department of Education of Jilin Province [2008] 296, 2011JTY05, 2011JTY10, 2011JTY11.

Notes and references

1 D. C. Reynolds, D. C. Look, B. Jogai, C. W. Litton, G. Cantwell and W. C. Harsch, *Phys. Rev. B: Condens. Matter*, 1999, **60**, 2340.

2 X. L. Wang, H. Zhu, Y. Bao, F. Yang and X. R. Yang, *ACS Nano*, 2011, **5**(4), 3250.
3 M. H. Huang, S. Mao, H. H. Q. Yan, Y. Y. Wu, H. Kind, E. Weber, R. Russo and P. D. Yang, *Science*, 2001, **292**, 1897.
4 M. Law, L. E. Greene, J. C. Johnson, R. Saykally and P. D. Yang, *Nat. Mater.*, 2005, **4**, 455.
5 X. D. Bai, E. G. Wang, P. X. Ago and Z. L. Wang, *Nano Lett.*, 2003, **3**, 1147.
6 F. Fang, D. X. Zhao, B. H. Li, Z. Z. Zhang and D. Z. Shen, *Phys. Chem. Chem. Phys.*, 2010, **12**, 6759.
7 F. Fang, D. X. Zhao, B. H. Li, Z. Z. Zhang, J. Y. Zhang and D. Z. Shen, *Appl. Phys. Lett.*, 2008, **93**, 233115.
8 B. J. Lokhande, P. S. Patil and M. D. Uplane, *Physica B*, 2001, **59**, 302.
9 P. Sharma, A. Gupta, K. V. Rao, F. J. Owens, R. Sharma, R. Ahuja, J. M. O. Guillen, B. Johansson and G. A. Gehring, *Nat. Mater.*, 2003, **2**, 673.
10 J. H. He, C. S. Lao, L. J. Chen, D. G. Davidovic and Z. L. Wang, *J. Am. Chem. Soc.*, 2005, **127**, 16376.
11 J. Fan and R. Freer, *J. Appl. Phys.*, 1995, **77**, 4795.
12 Y. F. Yan, M. M. Al-Jassim and S. H. Wei, *Appl. Phys. Lett.*, 2006, **89**, 181912.
13 Y. L. Li, X. Zhao and W. L. Fan, *J. Phys. Chem. C*, 2011, **115**, 3552.
14 G. L. Chai, C. S. Lin, J. Y. Wang, M. Y. Zhang, J. Wei and W. D. Cheng, *J. Phys. Chem. C*, 2011, **115**, 2907.
15 H. S. Kang, B. D. Ahn, J. H. Kim, G. H. Kim, S. H. Lim, H. W. Chang and S. Y. Lee, *Appl. Phys. Lett.*, 2006, **88**, 202108.
16 I. S. Kim, E. K. Jeong, D. Y. Kim, M. Kumar and S. Y. Choi, *Appl. Surf. Sci.*, 2009, **255**, 4011.
17 B. D. Ahn, H. S. Kang, J. H. Kim, G. H. Kim, H. W. Chang and S. Y. Lee, *J. Appl. Phys.*, 2006, **100**, 093701.
18 M. A. Thomas and J. B. Cui, *J. Phys. Chem. Lett.*, 2010, **1**, 1090.
19 A. E. Hichou, M. Addou, J. Ebothe and M. Troyonet, *J. Lumin.*, 2005, **113**, 183.
20 Z. D. Fu, Y. S. Cui, S. Y. Zhang, J. Chen, D. P. Yu, S. L. Zhang, L. Niu and J. Z. Jiang, *Appl. Phys. Lett.*, 2007, **90**, 263113.
21 Z. W. Pan, Z. R. Dai and Z. L. Wang, *Science*, 2001, **291**, 1947.
22 X. D. Bai, P. X. Gao, Z. L. Wang and E. G. Wang, *Appl. Phys. Lett.*, 2003, **82**, 4806.
23 Z. Q. Zhang, C. B. Jiang, S. X. Li and S. X. Mao, *J. Cryst. Growth*, 2005, **277**, 321.
24 W. S. Shi, O. Agyeman and C. N. Xu, *J. Appl. Phys.*, 2002, **91**, 5640.
25 T. B. Hur, Y. H. Hwang and H. K. Kim, *J. Appl. Phys.*, 2004, **96**, 1507.
26 A. N. Gruzintsev, V. T. Volkov, I. I. Khodos, T. V. Nikiforova and M. N. Koval'chuk, *Russian Microelectronics*, 2002, **31**, 200.
27 K. L. Liu, B. F. Yang, H. W. Yan, Z. P. Fu, M. W. Wen, Y. J. Chen and J. Zuo, *J. Lumin.*, 2009, **129**, 969.
28 C. Y. Geng, Y. Jiang, Y. Yao, X. M. Meng and J. A. Zapien, *Adv. Funct. Mater.*, 2004, **14**, 589.
29 Z. M. Liao, K. J. Liu, J. M. Zhang and J. X. Da, *Phys. Lett. A*, 2007, **367**, 207.
30 *Surfaces and Interfaces: Physics and Electronics*, ed. R. S. Bauer, North-Holland, Amsterdam, 1983.
31 D. C. Reynolds, D. C. Look and B. Jogai, *Phys. Rev. B: Condens. Matter*, 1998, **57**, 12151.
32 J. S. Jie, G. Z. Wang, Y. M. Chen, X. H. Han, Q. T. Wang and B. Xu, *Appl. Phys. Lett.*, 2005, **86**, 031909.
33 W. Y. Liang and A. D. Yoffe, *Phys. Rev. Lett.*, 1968, **20**, 59.
34 Y. R. Ryu and T. S. Lee, *Appl. Phys. Lett.*, 2003, **83**, 87.
35 M. A. Thomas and J. B. Cui, *J. Phys. Chem. Lett.*, 2010, **1**, 1090.